Maastricht University

In vivo assessment of the human cerebral microcirculation and its glycocalyx: A technical report

Document status and date:
Published: 01/06/2018

DOI:
10.1016/j.jneumeth.2018.03.009

Document Version:
Publisher's PDF, also known as Version of record

Document license:
Taverne

Please check the document version of this publication:

• A submitted manuscript is the version of the article upon submission and before peer-review. There can be important differences between the submitted version and the official published version of record. People interested in the research are advised to contact the author for the final version of the publication, or visit the DOI to the publisher's website.
• The final author version and the galley proof are versions of the publication after peer review.
• The final published version features the final layout of the paper including the volume, issue and page numbers.

Link to publication

In vivo assessment of the human cerebral microcirculation and its glycocalyx: A technical report

R.H.L. Haeren [a,*], K. Rijkers [a], O.E.M.G. Schijns [a,b], J. Dings [a,b], G. Hoogland [a,b], M.A.M.J. van Zandvoort [c,d], H. Vink [e], J.J. van Overbeeke [a,b]

[a] *Department of Neurosurgery, School for Mental Health and Neuroscience, Maastricht University Medical Center, Heerlen and Maastricht, The Netherlands*
[b] *Academic Center for Epileptology, Maastricht University Medical Center and Kempenhaeghe, Maastricht/Heeze, The Netherlands*
[c] *Department Molecular Cell Biology, School for Cardiovascular diseases CARIM and School for Mental Health and Neuroscience, Maastricht University, Maastricht, The Netherlands*
[d] *Institute for Molecular Cardiovascular Research IMCAR, RWTH Aachen University, Aachen, Germany*
[e] *Department of Physiology, School for Cardiovascular diseases CARIM, Maastricht University, Maastricht, The Netherlands*

HIGHLIGHTS

- The cerebrovascular glycocalyx might be a blood-brain barrier regulator.
- The cerebrovascular glycocalyx has only sparsely been reported on.
- We assessed the human cerebrovascular glycocalyx intraoperatively.
- Sidestream dark field imaging is a suitable technique to perform this assessment.
- A sterile slipcover required for cerebral assessment affects the results.

ARTICLE INFO

ABSTRACT

Introduction: The cerebral microcirculation and its glycocalyx, a matrix coating the luminal endothelium, are key regulators of capillary permeability and cerebral blood flow. Microvascular abnormalities are described in several neurological disorders. However, assessment of the cerebral microcirculation and glycocalyx has mainly been performed *ex vivo*.

New method: Here, the technical feasibility of *in vivo* assessment of the human cerebral microcirculation and its glycocalyx using sidestream dark field (SDF) imaging is discussed. Intraoperative assessment requires the application of a sterile drape covering the camera (slipcover). First, sublingual measurements with and without slipcover were performed in a healthy control to assess the impact of this slipcover. Subsequently, using SDF imaging, the sublingual (reference), cortical, and hippocampal microcirculation and glycocalyx were evaluated in patients who underwent resective brain surgery as treatment for drug-resistant temporal lobe epilepsy. Finally, vessel density, and the perfused boundary region (PBR), a validated gauge of glycocalyx health, were calculated using GlycoCheck© software.

Results: The addition of a slipcover affects vessel density and PBR values in a control subject. The cerebral measurements in five patients were more difficult to obtain than the sublingual ones. This was probably at least partly due to the introduction of a sterile slipcover. Results on vessel density and PBR showed similar patterns at all three measurement sites.

Comparison with existing methods: This is the first report on *in vivo* assessment of the human cerebrovascular glycocalyx. Assessment of the glycocalyx is an additional application of *in vivo* imaging of the cerebral microcirculation using SDF technique. This method enables functional analysis of the microcirculation and glycocalyx, however the addition of a sterile slipcover affects the measurements.

* Corresponding author at: Maastricht University Medical Center+, Department of Neurosurgery, PO Box 5800, 6202 AZ Maastricht, The Netherlands.
E-mail address: roel.haeren@mumc.nl (R.H.L. Haeren).

Conclusions: SDF imaging is a safe, quick, and straightforward technique to evaluate the functional cerebral microcirculation and glycocalyx. Because of their eminent role in cerebral homeostasis, this method may significantly add to research on the role of vascular pathophysiology underling various neurological disorders.

1. Introduction

In recent years, the study on the pathophysiology of neurological disorders has shifted from a traditional neuronal focus towards a more integrative paradigm that emphasizes cell–cell signaling (Guo and Lo, 2009). In particular, the interactions between the vascular and neuronal tissue have been of interest (Abbott et al., 2010; Brown and Thore, 2011; Farrall and Wardlaw, 2009; Rosenberg, 2012; Toth et al., 2017). Physiological brain function is highly dependent on adequate structure and function of the cerebral microcirculation due to the lack of energy reserves, an on average high and rapidly changing metabolic rate, and tight regulation of brain homeostasis (Abbott et al., 2010; Iadecola, 2004; Toth et al., 2017). Hence, interest in the cerebral microcirculation and the neurovascular interface rapidly increases.

The microcirculation regulates local blood flow to meet neuronal metabolic demands, a mechanism known as neurovascular coupling (Abbott et al., 2010; Iadecola, 2004; Muoio et al., 2014). Besides this, it orchestrates the rate of delivery and exchange of vital nutrients across the blood-brain barrier (BBB) (Abbott et al., 2010; Gould et al., 2016; Jacob et al., 2016; Taccone et al., 2010).

The BBB exerts its barrier function mainly by endothelial cells which are interconnected by tight junctions, and surrounded by the basal lamina, pericytes and astrocytes forming a stabilizing network (Abbott et al., 2010). Another significant barrier function may be exerted by the endothelial glycocalyx, further referred to as 'glycocalyx' (Haeren et al., 2016). This gel-like matrix covers the luminal side of the endothelium. An intact glycocalyx reduces interaction between the endothelium and blood components, and plays an important role in flow regulation as a mechanotransductor (Ebong et al., 2014; Reitsma et al., 2007). Consequently, the glycocalyx is a key regulator of vascular permeability, cerebral blood flow, capillary perfusion, and cell adhesion (Haeren et al., 2016; Megens et al., 2007; Rahbar et al., 2015). Preservation of an intact glycocalyx is an important aspect of vascular health. Not surprisingly, many vascular diseases and related risk factors like stroke, renal failure, sepsis, hypertension, and diabetes mellitus are associated with a disturbed glycocalyx (Becker et al., 2010; de Mesy Bentley, 2011; Martens et al., 2013; Ostrowski et al., 2013; Singh et al., 2011; Vlahu et al., 2012).

Imaging and assessment of the human cerebral microcirculation and its glycocalyx has mainly been performed *ex vivo* by microscopic evaluation of structural changes and analysis of vascular (wall) stainings and markers (Hunsberger et al., 2005; Kastanauskaite et al., 2009; Morin-Brureau et al., 2011; Pitkänen and Lukasiuk, 2009; Rigau et al., 2007). However, functional analysis of the microcirculation cannot be performed *ex vivo*. Nowadays, non-invasive imaging techniques, including sidestream dark field (SDF) imaging, allow *in vivo* assessment of the microcirculation and glycocalyx. SDF imaging has mainly been performed to assess the sublingual microcirculation (Dane et al., 2015; Martens et al., 2013; Vlahu et al., 2012). Recently, SDF imaging and its technical predecessor have also been used to assess the cerebral microcirculation (Mathura et al., 2001; Uhl et al., 2003; Pennings et al., 2004, 2006a,b, 2009; Wan et al., 2009; Pérez-Bárcena et al., 2011, 2015). These studies assessed microvascular parameters such as vessel density and flow velocity in patients undergoing cranial surgery

for by example aneurysm clipping or decompressive surgery. However, *in vivo* analysis of the cerebrovascular glycocalyx has not been performed to date. The addition of specific software to SDF imaging is assumed to enable assessment of the cerebrovascular glycocalyx (Haeren et al., 2016).

We have developed a prospective observational case-control study in which the human sublingual, cortical, and hippocampal microcirculation and glycocalyx were assessed *in vivo* by SDF imaging. Intraoperative use of the SDF camera required adding a sterile slipcover.

The intention of this study was to evaluate cerebral microvascular and glycocalyx properties in epilepsy patients. Microvascular abnormalities and BBB dysfunction have previously been associated with the pathophysiology of epilepsy (Alonso-Nanclares and DeFelipe, 2014; Heinemann et al., 2012; Kastanauskaite et al., 2009; Parfenova et al., 2005; Rigau et al., 2007; van Vliet et al., 2014). In this paper, the technical feasibility of *in vivo, i.e.* during brain surgery, assessment of the cerebral microcirculation and its glycocalyx in epilepsy patients is discussed.

2. Material and methods

This study was approved by the local medical ethical committee (METC azM/UM) and complies with the Declaration of Helsinki and principals of Good Clinical Practice. This study has been registered at The Netherlands National Trial Register (ID: NTR 5568). The study protocol was published recently (Haeren et al., 2017). Patients were included upon obtained informed consent.

2.1. Participants

Included epilepsy patients were mentally competent patients between 18 and 60 years of age who were candidates for epilepsy surgery because of chronic drug-resistant temporal lobe epilepsy (TLE) as was revealed by thorough preoperative examination. Surgical treatment included anterior temporal lobectomy plus amygdalohippocampectomy. Exclusion criteria were pregnancy, history of hypertension, diabetes mellitus, hyperlipidemia, stroke or other cardiovascular diseases, use of cardiovascular medication, or signs of cerebral small vessel disease on cerebral MRI.

Since intraoperative assessment of the cerebral microcirculation requires the application of a sterile drape covering the camera (slipcover), one healthy control was included to compare sublingual measurements with and without sterile slipcover.

2.2. Imaging procedures: videomicroscopy

Measurements were performed using a Capiscope videomicroscope camera (KK Technology; Honiton, UK). This handheld camera is based on SDF technique. The camera contains a central light guide that is surrounded by concentrically placed light emitting diodes (LEDs) emitting light at a wavelength of 530 nm, which is absorbed by (des-)oxyhemoglobin in erythrocytes. Consequently, erythrocytes appear as dark disks on a grayish background. The light is re-emitted *via* the central light guide towards the objective lens providing an image of the illuminated area. Images of 752×480 pixels are collected with a $5\times$ objective at 30 frames per

second. Spatial resolution of the images is 0.91 μm per pixel. To reduce operator-related variability, all images were acquired by the same investigator (RH).

2.3. Imaging procedure protocol

In patients, one sublingual (M1) and two cerebral (cortically (M2) and hippocampally (M3)) were included. The sublingual measurement, performed directly following the induction of general anesthesia, served as a validated reference, as most reports on microcirculation assessment using SDF imaging are performed sublingually (Martens et al., 2013; Nieuwdorp et al., 2008; Vlahu et al., 2012). At each measurement, systolic and diastolic blood pressure, and heart rate were recorded. For the cerebral measurements, the SDF camera is enclosed within a sterile slipcover (Camera Drape with EZ SERT, Microtek Medical Inc).

To assess the potential effect of the slipcover on the outcome parameters, a healthy control subject underwent sublingual measurements both, with (n = 15) and without (n = 15) a sterile slipcover in the morning after an overnight fast. Measurements were performed in alternating (with or without sterile slipcover) blocks of five measurements. This result is discussed before those obtained from patients in order to adequately take the patient's results into account.

2.4. Measurement parameters

For each measurement, at least 10 recording sites and a minimum of 3000 microvessel segments were selected automatically. A recording site is defined as a tissue surface location where on average 300 microvessel segments were selected for recording. This selection only takes place when focus, contrast, and image quality are within predefined acceptable ranges, with as a prerequisite that the camera does not move simultaneously. Of these, obtaining adequate focus is performed manually by turning the rotary knob on the camera thereby altering the focus point of the lens. A microvessel segment is defined as a segment of 10 μm along the length of a selected vessel. Next, a sequence of 40 frames containing around 300 microvessel segments is recorded in time thereby fulfilling the criteria for a measurement site. Recording is continued until at least 10 sites and 3000 microvessel segments are included. As the tissue and camera move over time, the measurement sites contain various microvessel segments.

During this procedure, pressure artefacts were avoided by placing the camera on the tissue surface while maintaining red blood cell flow in the microvessels. In addition, artefacts by blood clots were reduced by rinsing the cerebral tissue before measurement using 37 °C Ringer's lactate.

GlycoCheck © software was used to select and measure the width of the red blood cell column (RBCC) in vessel segments with median RBCC widths ranking from 5 to 20 μm. RBCC width is calculated in all microvessel segments. As mentioned, each vessel segment has a length 10 μm. The software automatically places twenty-one line markers at an interval of 0,5 μm along all segments. The RBCC width is measured at all single line markers. Since each segment is recorded as a sequence containing 40 frames, a total of 840 RBCC widths are included per vessel segment. Subsequently, the median RBCC width for each vessel segment is calculated based on these 840 RBCC widths.

Determination of the vessel diameter is difficult in these small vessels since erythrocytes are visualized, but not the vessel wall. As the reported diameters correspond to the median RBCC diameter of a certain vessel, they are an underestimation of actual anatomic vessel diameter.

Dane et al. have described the above-mentioned measurement parameters in more detail, including a validation study and images illustrating vessel analysis in adequate magnification (Dane et al., 2014).

2.5. Outcome parameters

Functional vessel density is defined as the number of microvessels for each RBCC diameter class per mm^2 and was automatically determined by the Glycocheck © software.

The glycocalyx is also evaluated using Glycocheck © software. Since compression of a 'healthy' glycocalyx by erythrocytes is limited, an exclusion zone between the RBCC and endothelium is apparent. This exclusion zone forms the basis of glycocalyx analysis. However, when using SDF imaging the exclusion zone cannot be determined as the vessel wall (endothelium) is not visualized. Therefore, the perfused boundary region (PBR) is used as a surrogate gauge of glycocalyx stability and thickness. The PBR is the outermost luminal part of glycocalyx that is slightly permeable for erythrocytes. Hence, the PBR is based on the variations of RBCC width in each vessel segment. To calculate the PBR, one should first determine the total perfused diameter (Dperf). The Dperf is calculated by linear regression analysis of the slope between the 25th and 75th RBCC width percentiles of each vessel segment (Dane et al., 2014; Martens et al., 2013). The point where this line intersects with the x-axis is a reliable marker (when including all 840 measurements) if the most outward location of the RBCC, i.e. the Dperf. The PBR is defined as the distance between the RBCC width and Dperf and is present on both sides of the RBCC. The PBR, expressed in micrometers (μm) is thus calculated as follows: PBR = (Dperf − median RBCC width)/2.

Calculation of Dperf and PBR strongly depend on the measurement of the median RBCC width. To ensure that these measurements are independent of red blood cell filling of the vessel segments (hematocrit), the software only includes vessel segments that have a filling percentage of more than 50%. Hence, vessel segments are only selected when at least 11 of the 21 line markers have a positive signal for the presence of an erythrocyte. Being independent of hematocrit, increased Dperf and PBR values reflect an unstable or damaged glycocalyx that is more accessible for erythrocytes.

2.6. Data and statistical analysis

All relevant clinical and measurement data were recorded in a secured and encoded database. Clinical and procedural parameters are presented as mean ± standard error of mean (SEM). The sublingual measurements with and without sterile slipcover to assess the effect of slipcover were compared using paired T-tests. Results of vessel density and PBR of the sublingual, cortical and hippocampal microcirculation are presented as mean ± SEM and are illustrated in graphs per RBCC diameter. The predictive value of the sublingual PBR for cortical and hippocampal PBR is calculated using Pearson correlation coefficient. Calculations were performed using SPSS (IBM, SPSS Statistics for Windows, version 20.0, 2011).

3. Results

3.1. General patient characteristics

A total of five TLE-patients with a mean age of 44.4 years were included in this study. Further clinical details are summarized in Table 1. All measurements were performed after an overnight fast which was required for anesthesia induction. Assessment of the sublingual and hippocampal microcirculation was completed in all patients, while the cortical measurements were accomplished in 4 TLE-patients.

Table 1
Clinical and surgical data of TLE-patients.

	Sex	Age (years)	BMI (kg/m^2)	Smok	Indication	Side	Cortical site	PA	HS type	FCD type
P1	F	26	25.6	N	TLE	R	STG	Hippocampal sclerosis	1	N/A
P2	F	46	26.9	N	TLE	L	STG	Hippocampal sclerosis	2	N/A
P3	F	50	25.6	N	TLE	R	STG	Hippocampal sclerosis	1	N/A
P4	M	47	28.1	N	TLE	R	STG	No abnormalities	N/A	N/A
P5	F	53	25.5	N	TLE	L	STG	Meningioma and DNET	N/A	N/A

In this table, clinical and surgical data of the included TLE-patients are summarized.
BMI: body mass index, DNET: dysembryoplastic neuroepithelial tumor, F: female, FCD type: type of (focal) cortical dysplasia, HS type: type of hippocampal sclerosis according to ILAE classification, L: left, M: male, N: no, N/A: non-applicable, R: right, Smok: smoking, PA: results of histopathological examination, SFG: superior frontal gyrus, Side: side of surgery/measurement, STG: superior temporal gyrus, Y: yes.

Table 2
Clinical and technical measurement characteristics.

	SBP ± SEM (mmHg)	DBP (±SEM) (mmHg)	HR ± SEM (per minute)	Duration (seconds)	Recording sites	Microvessel segments
M1 (n = 5)	95.4 ± 3.8	59.4 ± 5.1	62.8 ± 3.9	40.0 ± 6.3	16.0 ± 1.1	3287.4 ± 27.0
M2 (n = 4)	111.0 ± 4.6	55.0 ± 1.2	58.5 ± 3.6	141 ± 65.9	27.5 ± 2.3	3263 ± 44.8
M3 (n = 5)	112.2 ± 7.7	61.4 ± 3.9	65.2 ± 5.4	115.8 ± 39.0	27.0 ± 5.0	3213.0 ± 70.7

Hemodynamic parameters (SBP, DBP and HR) were recorded during each measurement. Besides a slightly lower SBP in M1 and DBP in M2, hemodynamics parameters were comparable between measurements. The duration of the cerebral measurements, M2 and M3, was substantially longer than those of the sublingual measurements. Each measurement required at least 3000 microvessel segments. As a result, the number of recordings was higher for cerebral measurements (M2 and M3) than for sublingual measurements.
DBP: diastolic blood pressure, HR: heart rate, M1: sublingual measurements, M2: cortical measurements, M3: hippocampal measurement, SBP: systolic blood pressure, SEM: standard error of mean.

Hemodynamic parameters for each measurement are presented in Table 2. In this table, the duration of each assessment is also provided. Mean time for sublingual microcirculation (M1) assessment was 40.0 s. The duration of the cortical (M2) and hippocampal (M3) measurements was substantially longer with a maximum of 6 and 4 min, respectively. The number of recordings to include at least 3000 microvessel segments was markedly higher in M2 and M3.

3.2. Imaging procedure in patients

Directly following anesthesia induction and intubation with fixation of the endotracheal tube by adhesive plaster, sublingual measurements were carried out. Study subjects were in supine position and the camera was brought in orally along the endotracheal tube (Fig. 1A). The central sublingual surface area was chosen for examination.

Next, incision, craniotomy, and durotomy were performed according to site of surgery and surgeon's preference. When the cortex was in view, the tip of the camera was wettened in Ringer's lactate and enclosed with the sterile slipcover. Blood clots were rinsed off the cortex surface using warm Ringer's Lactate. Finally, the camera was gently placed on the surface of temporal cortex (Fig. 1B) and subtly fixed by the neurosurgeon to minimize pressure and movement artefacts. In contrast to sublingual measurements, this was a rather time-consuming procedure in cortical measurements.

Anterior temporal lobe resection was performed subsequently. When the hippocampus was fully visualized, blood clots were rinsed off using warm Ringer's lactate. Thereafter, the camera with sterile slipcover was gently placed on the lateral surface of the hippocampus and loosely fixed by the neurosurgeon (Fig. 1C). Fig. 2A and B, and Video 1 (in the Supplementary material) show images of the microcirculation.

3.3. Imaging procedure: issues and solutions

In the first participant, we were not able to adequately visualize the cortical microcirculation. During this measurement, air bubbles
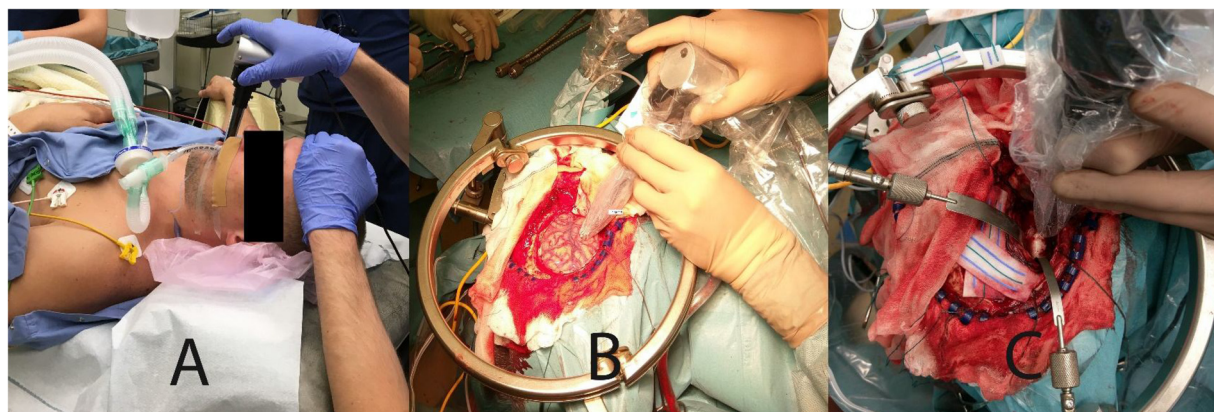
Fig. 1. This figure exemplifies the position of the patient, measurement site, and handling of the Capiscope camera during the measurement of the central sublingual surface (A), the outer temporal cortical surface (B), and the lateral hippocampal surface (C). In A, the tip of the camera is placed alongside the endotracheal tube. The rotary knob near the handgrip is used to obtain adequate focus. During the cortical (B) and hippocampal (C) measurement, the camera is enclosed in the sterile slipcover. One hand is placed around the camera tube to stabilize the camera and reduce movement artefacts. The other hand is used to obtain adequate focus. In Fig. 1C, the white structure at the tip of the camera is the hippocampus. This structure is situated deeply within the cranium at the most mesial part of the temporal lobe.
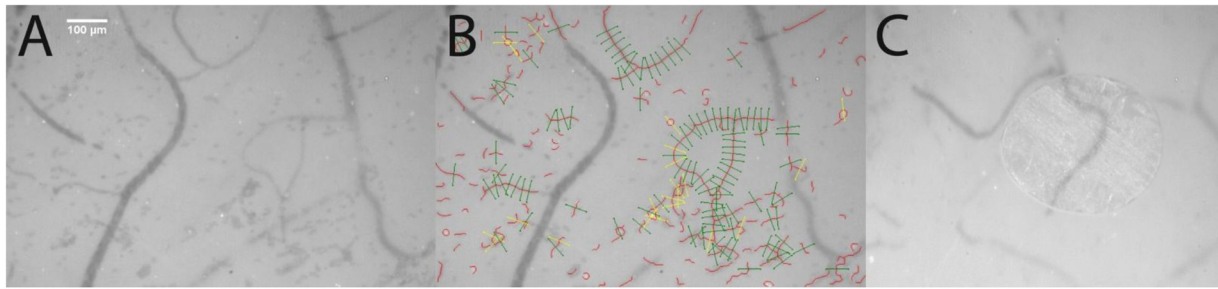
Fig. 2. Visualization of the hippocampal microcirculation as shown by SDF imaging (A). In Fig. 2B, the similar image is depicted while analysis is performed using Glycocheck © software. Here, red lines indicate the vessels that are recognized by the flow of erythrocytes. The red blood cell column (RBCC) width variation is then estimated based on the green and yellow lines that are placed perpendicular on the vessels. These green and yellow lines indicate 10 μm vessel segments within the vessel. Green lines reflect vessel segments that recognized red blood cells in >50% of its line markers and were therefore included in further calculations. The yellow lines indicate vessels segments that were excluded due to red blood cell filling percentage <50% or due to a poor signal to noise ratio. Fig. 2C shows an air bubble obstructing the software to recognize vessels, despite adequate focus. (For interpretation of the references to colour in this figure legend, the reader is referred to the web version of this article.)

were encountered in the slipcovered tip of the camera, obstructing acquisition of adequate focus to assess the microcirculation (Fig. 2C). We assumed that the introduction of the sterile slipcover enclosing the camera enabled air bubbles to enter in between, even though the tip of the camera was wettened in Ringer's lactate before it was enclosed by the slipcover. Therefore, the conducting and pasting substance between the camera and slipcover was altered to sterile gel (Aquasonic sterile ultrasound transmission gel, Parker laboratories, Fairfield, USA). In the subsequently performed sterile hippocampal measurement, no air bubbles were noted. All following measurements were successfully completed using the gel instead of water. Nevertheless, we noted that it was sometimes difficult to properly visualize the cortical and hippocampal microcirculation and obtaining adequate focus appeared time consuming, independently of learning curve.

No (serious) adverse events were recorded during the measurement procedures or surgery.

3.4. Microvascular density

3.4.1. Results in control subject: effect of slipcover

Sublingual vessel density was affected by the slipcover, *i.e.* a lower total number of vessels was detected when the sterile slipcover was placed over the camera compare to measurements without a slipcover, 296 ± 18 and 381 ± 26 respectively ($p = .009$). In particular, a significant reduction of the smaller microvessels, *i.e.* RBCC diameter classes 6–10, was noted (see Fig. 3).

3.4.2. Results in patients

The sublingual measurement was completed in all five participants. Mean sublingual vessel density was 274 ± 47 per mm². Mean cortical vessel density (n = 4) and hippocampal vessel density (n = 5) were substantially lower compared to the sublingual vessel density, 144 ± 21 per mm² and 193 ± 47 per mm², respectively. In Fig. 4, microvascular density per RBCC diameter is presented. Mean sublingual vessel density is increased for all RBCC diameters when compared to the cortical and hippocampal vessel density. All three sites show a similar pattern, with a vessel increase of 7–10 μm RBCC diameter classes.

3.5. Perfused boundary region

3.5.1. Results in control subject: effect of slipcover

The calculated PBR was affected by the introduction of the slipcover as well. The overall mean PBR increased from 1.93 ± 0.07 μm to 2.20 ± 0.06 μm in the measurements without and with slipcover, respectively ($p = .004$). This was mainly due to significantly higher PBR values in the larger RBCC diameter classes of 13–20 μm, with

the exception of the nearly significant ($p = .057$) increase in RBCC diameter class of 16 μm. The results are presented in Fig. 5.

3.5.2. Results in patients

The mean sublingual PBR (n = 5) was 1.85 ± 0.19 μm. The mean cortical PBR of the successfully assessed four patients was evidently increased, 2.28 ± 0.18 μm. The mean hippocampal PBR (n = 5, TLE-patients) was 2.01 ± 0.13 μm. Mean PBR values per RBCC diameter of all three sites are illustrated in Fig. 6. This figure shows incremental PBR values in increasing vessel diameters.

3.6. Predictive value of the sublingual measurements

As can be seen in Fig. 7 (graphs A-C-E-G-I), high intra- and interindividual variation was found between sublingual, cortical, and hippocampal vessel densities. No correlation was found between the sublingual and cortical (Pearson correlation 0.425, $p = .58$) or hippocampal (Pearson correlation −0.491, $p = .40$) PBR values (Fig. 7, graphs B-D-F-H-J).

4. Discussion

In this study, we have described a method to assess the human cerebral microcirculation and its glycocalyx during a craniotomy. Using SDF imaging, the cerebral microcirculation can be visualized easily, safely, and quickly. Subsequent analysis by Glycocheck © software, enabled us to analyze the cerebrovascular glycocalyx.

Measurements are affected by the slipcover that is required for sterile cerebral measurements. The preliminary results on vessel density and PBR presented here, are provided to illustrate the feasibility of *in vivo* measurements on cortical and hippocampal tissue.

### 4.1. Evaluation of the slipcover effect

As comes clear from Figs. 3 and 6, the addition of a slipcover affects the results for vessel density and PBR values. Regarding vessel density, a reduced vessel density is noted when the camera is enclosed by the sterile slipcover. This 'slipcover effect' is most pronounced for the recognition of the smallest vessels, *i.e.* with a RBCC diameter of 10 μm or smaller. This effect might be due to loss of adequate focus when the slipcover is introduced. The slipcover alters fraction of the emitted and re-emitted light impeding adequate focus. In addition, the slipcover disturbs image quality reducing the recognition of the smallest microvessels in particular. In line with the cerebral measurements, the sublingual measurements performed with the sterile slipcover also included sterile transmission gel (Aquasonic sterile ultrasound transmission gel, Parker laboratories, Fairfield, USA) between the slipcover and cam-

Sublingual vessel density
with versus without slipcover
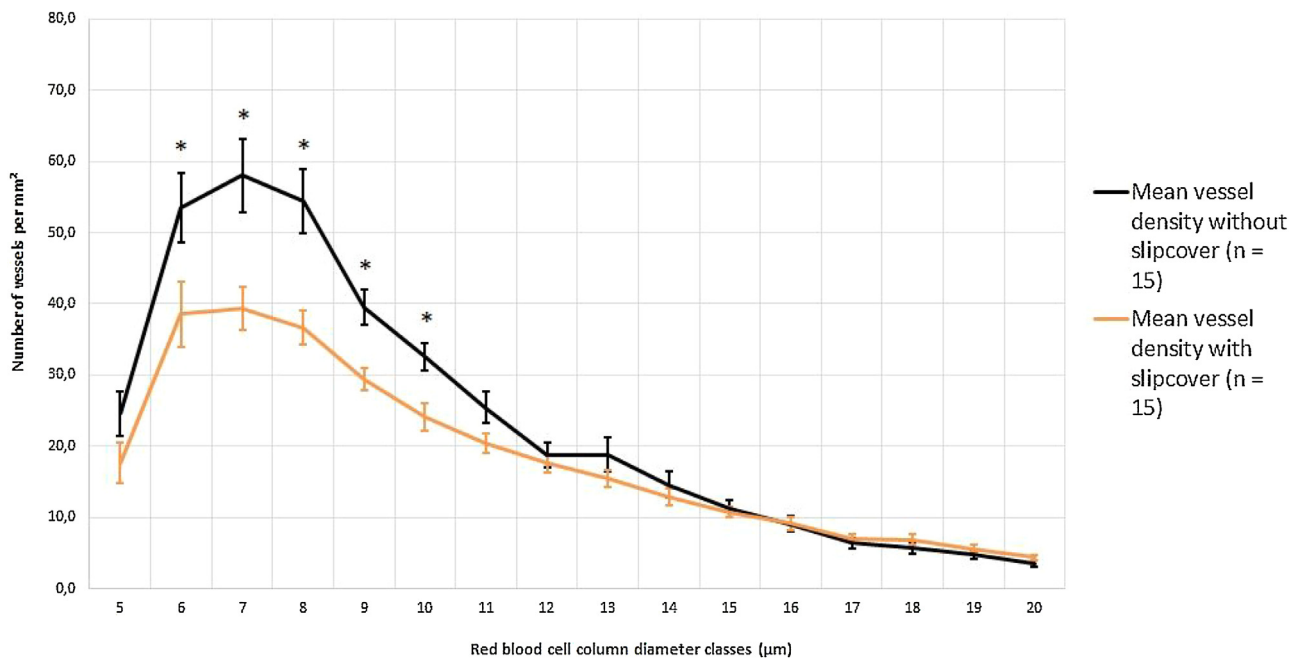
Fig. 3. In this figure, the red blood cell column (RBCC) width is presented per diameter classes on the X-axis. The mean number of microvessels recognized for each RBCC diameter class is illustrated on the Y-axis. The sublingual measurements without a slipcover are illustrated by the black line, whereas the orange line indicates the sublingual measurements with a slipcover. Clearly, the number of vessels recognized is reduced after introduction of the slipcover. For RBCC diameters classes 6–10 μm, these differences are significant. Error bars shown reflect the standard error of mean. * p-value < .05. (For interpretation of the references to colour in this figure legend, the reader is referred to the web version of this article.)

Microvascular density
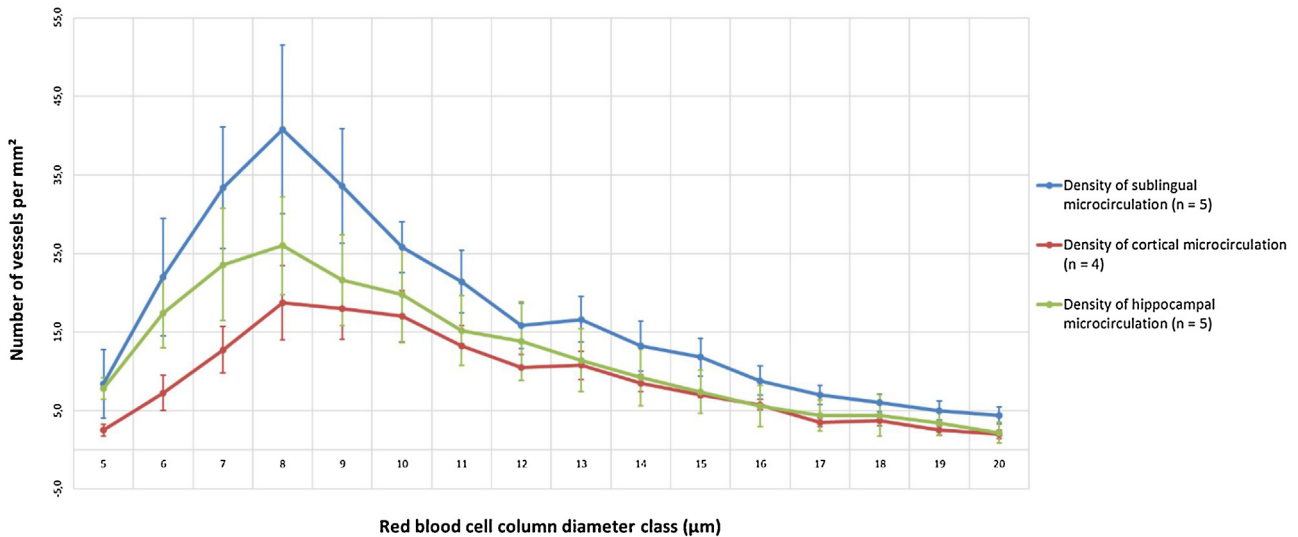
Fig. 4. Mean ± standard error of mean number of microvessels are expressed per red blood cell column (RBCC) diameter class, reflecting microvascular density. The sublingual (blue line) microvascular density is evidently higher for all RBCC diameters than the microvascular density of the hippocampus (green line) and cortex (red line). Note that the density of vessels up to 8 μm is substantially lower in the cortex than in the hippocampus. (For interpretation of the references to colour in this figure legend, the reader is referred to the web version of this article.)

era tip. The presence of this gel further complicates light fraction and image quality.

As mentioned, the software only selects vessel segments when focus, contrast, and image quality are within predefined acceptable ranges. When the images are in near-focus, the smallest vessels are not recognized and do not acquire the required fill-ing percentage due to lack of focus. Larger vessels are less sensitive to this effect, as these vessels are already selected when the images are in near-focus. This would explain why the introduction of the slipcover leads to a low density of smaller microvessels, whereas it does not affect density of larger microvessels.

Sublingual PBR values
with versus without slipcover
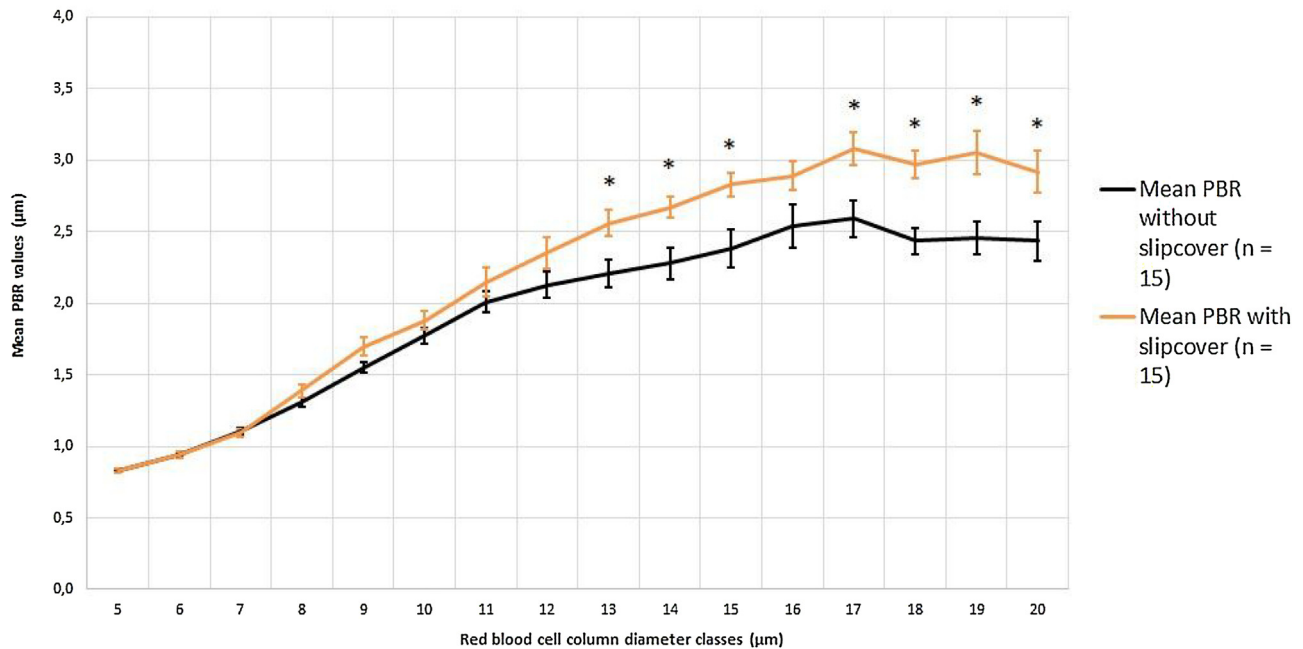
Fig. 5. In this figure, mean perfused boundary region (PBR) values are presented for each red blood cell column diameter (RBCC) diameter classes. The sublingual measurements without a slipcover are illustrated by the black line, whereas the orange line represents the sublingual measurements with a slipcover. With increasing RBCC diameter classes, increased PBR values are noted in the measurements performed with a slipcover. These values were significantly higher for RBCC diameters classes 13–15 μm and 17–20 μm. Error bars shown reflect the standard error of mean. * p-value < .05. (For interpretation of the references to colour in this figure legend, the reader is referred to the web version of this article.)

Microvascular perfused boundary region
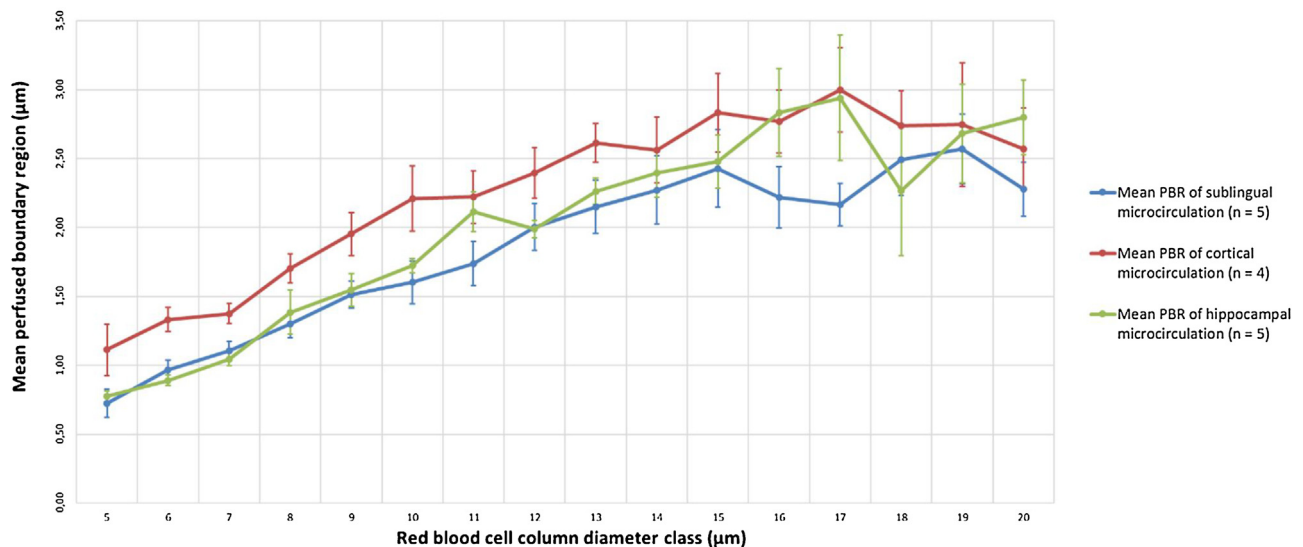
Fig. 6. Mean ± standard error of mean perfused boundary region (PBR) values are expressed peris presented red blood cell column (RBCC) diameter classes. Sublingual (blue line), cortical (red line), and hippocampal (green line) PBR values tend to increase with increasing RBCC diameter. The PBR values of the cortical microcirculation are slightly increased between RBCC diameters of 5 and 15 μm when compared to both, sublingual and cortical PBR values. (For interpretation of the references to colour in this figure legend, the reader is referred to the web version of this article.)

If the same holds true for cerebral measurements, the 'slipcover-associated' reduced number of recognized (smaller) microvessels will lead to an increase in the number of recordings required to obtain at least 3000 vessel segments. This is indeed in line with our observation that vessel density of the cortical and hippocampal (smaller) microcirculation was lower than sublingually and the number of recordings were markedly increased for the cerebral measurements.

In contrast to the above described effects on vessel density, the effect of the slipcover on PBR values is mainly apparent in
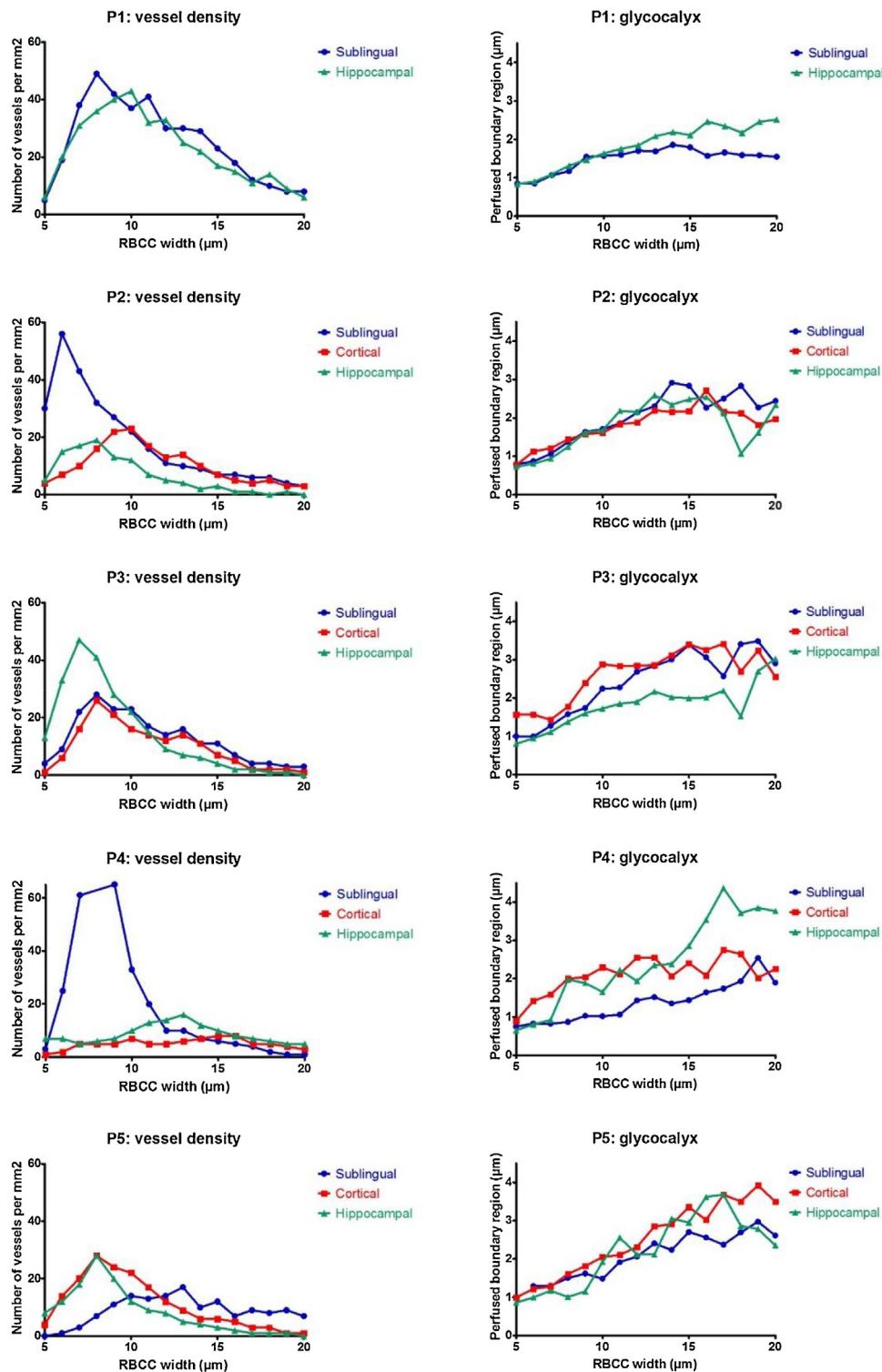
Fig. 7. In the graphs on the left, vessel density per red blood cell column(RBCC) width of the sublingual (blue), cortical (red), and hippocampal (green) microcirculation are specified per patient. There is high intra- and interindividual variation between densities of these sites. The perfused boundary region (PBR) per RBCC width are also specified per patient. Incremental PBR values for increasing RBCC width can be noted, although no statistical correlation was found between the sublingual (blue), cortical (red), and hippocampal (green) PBR. (For interpretation of the references to colour in this figure legend, the reader is referred to the web version of this article.)

larger microvessels, *i.e.* microvessels with RBCC diameters ranging 13–20 μm. We believe this is the result of inclusion of both in-focus and near-focus images. Despite the inclusion of near-focus images, in-focus images were still acquired. This can be deduced from the vessel density results as the vessel density of the smallest microvessels was reduced but was not zero. As mentioned, recognition of the

smallest vessels requires in-focus images indicating that the number of in-focus images was reduced but not zero. As the smallest vessels were recognized on in-focus images, PBR values were adequately calculated by the software. Consequently, the PBR values of the smallest microvessels were comparable. On the contrary, larger microvessels are also recognized in near-focus images. Their vessel

density is therefore independent of the presence or absence of the sterile slipcover. However, recognition of variations in RBCC width is still affected in the larger microvessels included from the near-focus images. This alters the calculation of Dperf and PBR resulting in increased PBR values.

In summary, the introduction of the slipcovers reduces the number of recognized microvessels, in particular the smaller microvessels, and results in increased PBR values, in particular in the larger microvessels. This should be taken into account in future experiments when a slipcover is introduced.

4.2. Evaluation of imaging procedure in patients

In general, visualization of the sublingual, cortical, and hippocampal microcirculation using SDF imaging is a safe technique that does not significantly prolong surgery or affects sterility. However, the sterile cerebral measurements were more difficult to obtain when compared to the sublingual. The entry of air bubbles between the camera and the sterile slipcover can be prevented by using a gel as pasting conductor. Nevertheless, the time to obtain adequate focus that was required to start data recording for cerebral measurements varied from 30 s up to 6 min. We assume that this is mainly due to the introduction of the sterile slipcover requiring more measurement sites as discussed above. Additionally, physiological pulsations of the brain and cerebrospinal fluid that are not present sublingually may have contributed to the prolonged duration of cerebral measurements.

4.3. Microvascular density in patients

Assessment of the human cerebral microcirculation has mainly been performed *ex vivo* by histologic evaluation (Kastanauskaite et al., 2009; Morin-Brureau et al., 2011; Pitkänen and Lukasiuk, 2009; Rigau et al., 2007). *Ex vivo* assessment does not allow functional analysis of the microcirculation. Recently, SDF imaging and similar videomicroscopy techniques have been used to evaluate the human cerebral microcirculation (Mathura et al., 2001; Pennings et al., 2006a,b, 2009, 2004; Pérez-Bárcena et al., 2015, 2011; Uhl et al., 2003). In our study, we have confirmed these results by visualizing the sublingual, cortical, and hippocampal functional microcirculation and analyzing microvascular density. The sublingual vessel density was substantially higher than that in the hippocampus and even more so compared to that in the cortex. As was pointed out above, this is partly due to the introduction of the sterile slipcover altering image acquisition properties.

Yet, when comparing the two sterile cerebral measurements, vessel density of the smallest microvessels is higher in the hippocampal than in the cortical microcirculation. This difference cannot be explained by the slipcover, as both measurements were performed using the slipcover. To discuss whether this is a physiological or pathophysiological finding is difficult due to the low number of included patients thus far.

We have tried to compare our results on the human cerebral vessel density to other reports using SDF imaging or its technical predecessor. However, most of these reports have mainly assessed parenchymal arterioles and venules with larger diameters (Mathura et al., 2001; Pennings et al., 2004, 2006a,b, 2009). We found two reports on the vessel density of the cortical microcirculation defined as RBCC diameters of 10–100 μm (Pérez-Bárcena et al., 2015, 2011). Vessel density was expressed as perfused vessel density defined as the length (in millimeter) of perfused vessels of all diameters per mm². The median perfused vessel density was 6.16 per mm² in control subjects, compared to 2.77 per mm² in stroke patients (Pérez-Bárcena et al., 2011). In patients with traumatic brain injury, mean perfused vessel density was 6.5 per mm² (Pérez-Bárcena et al., 2015). To calculate the total length of per-

fused vessels for our data, we have to multiply the total number of vessel segments with 10 (each vessel segment has a length of 10 μm). Next, the total length of perfused vessels in μm needs to be divided by 1000 to express the length in millimeters. Doing so, the mean perfused vessel density of the cortical microcirculation was 1.44 per mm². In our study, microvessel between 5 and 20 μm were included whereas Pérez-Bárcena et al. included vessel between 10 and 100 μm. This probably explains the low perfused vessel density of the cortical microcirculation in our study. In addition, microvascular density was also affected by the slipcover as explained above.

In our study, the distribution of RBCC diameters was comparable between all three sites with a predominant peak in the range of 7–10 μm. As this is the first study characterizing cerebral microvascular densities at different cerebral parenchymal sites and comparing them to sublingual densities, we cannot relate these findings to other reports. Noteworthy, a similar peak was also found in the sublingual microcirculation of the control subject.

When sublingual vessel density would be comparable or correlated to cortical and/or hippocampal vessel density, the assessment of the sublingual microcirculation would suffice to predict cerebral microvascular densities. However, we found high intra- and interindividual variation of site-specific vessel densities reducing the predictive value of the sublingual measurement.

4.4. Perfused boundary region in patients

The glycocalyx is a matrix covering the luminal side of the endothelial cells. It consists of proteoglycans and glycoproteins that provide a network in which other plasma- or endothelium-derived molecules are incorporated (Haeren et al., 2016). The endothelial side of the glycocalyx is more stable and firmly connected to the endothelium, whereas the luminal side is more dynamic and permeable for blood components like erythrocytes (Haeren et al., 2016; Reitsma et al., 2007). The PBR reflects this dynamic and permeable part of the glycocalyx interacting with erythrocytes. During inflammation or in cardiovascular disease, the glycocalyx is damaged and unstable which is characterized by a more dynamic and accessible glycocalyx that is reflected by an increased PBR. Consequently, an increase of the RBCC width variation and PBR can be detected. Thus, small PBR values illustrate health and stability of the glycocalyx. As PBR is the results of interactions with erythrocytes, the number of erythrocytes within the blood (hematocrit) can affect PBR values. In our study, this is taken into account by only including vessels segments with a filling percentage >50% thereby ensuring adequate RBCC width calculations.

Mean sublingual PBR of the TLE-patients was comparable to the author's mean sublingual PBR values when measured without the slipcover, $1.85 \pm 0.19\,\mu m$ versus $1.91 \pm 0.07\,\mu m$, respectively. These results are also comparable to sublingual PBRs in healthy controls as previously reported by Dane et al. and Martens et al., who found an average of $1.85 \pm 0.20\,\mu m$ (n = 10) and $2.08 \pm 0.24\,\mu m$ (n = 19), respectively (Dane et al., 2014; Martens et al., 2013). In these studies, microvessels with RBCC widths of 5–25 μm were included.

Cerebrovascular glycocalyx thickness has only sparsely been evaluated. Most reports have assessed this glycocalyx using *ex vivo* techniques. It is well known that *ex vivo* measurements of the glycocalyx underestimates its actual thickness due to collapse of the glycocalyx in *ex vivo* conditions. To the best of our knowledge, there is only one report on the *in vivo* thickness of the cerebrovascular glycocalyx (Yoon et al., 2017). In this study, the cerebrovascular glycocalyx was evaluated in healthy mice by making a cranial window including durotomy. Fluorescent wheat germ agglutinin lectins were used to label various components of the glycocalyx and were evaluated using two-photon laser scanning microscopy.

The mean glycocalyx thickness within capillaries (ranging 3–5 μm) was 0.42 ± 0.02 μm and 1.15 ± 0.03 μm in parenchymal arterioles (ranging 10–25 μm). Hence, the capillary glycocalyx thickness is smaller than the PBR values for the smallest microvessels in our study. This might be related to the inclusion of smaller vessels (ranging 3–5 μm) in the study by Yoon et al., whereas the lowest RBCC width in our study was 5 μm. As mentioned, RBCC width is an underestimation of vessel diameter. That does however not explain why the mean glycocalyx thickness of parenchymal arterioles is also lower than our PBR values in similar sized microvessels. This is probably due to underestimation of the actual glycocalyx thickness when using wheat germ agglutinin lectins, as these lectins only label specific glycocalyx components, like heparan sulfate and hyaluronan (Haeren et al., 2016). Moreover, cerebrovascular glycocalyx components and thickness in mice may differ from those of humans.

Naturally, PBR values gradually increase with increasing vessel diameter, which is confirmed in our sublingual and cerebral observations. These observations also demonstrate that PBR values seem to reach a plateau from a RBCC width of 15 μm upwards. The glycocalyx thickness, and hence PBR values, has been related to shear stress levels (Yoon et al., 2017). Capillaries receive low shear stress due to low blood flow velocity and small vessel diameter. Hence, they are characterized by a thinner glycocalyx layer. In contrast, larger parenchymal arterioles with higher blood flow velocities experience higher shear stress and have a thicker glycocalyx layer. The plateau probably reflects comparable levels of shear stress within the larger microvessels (arterioles).

Furthermore, we found that PBR values of the sublingual and hippocampal microcirculation were rather well comparable, while cortical PBR values appeared to be increased between 5 and 15 μm RBCC widths. This difference cannot be explained by the 'slip-cover effect', as this effect mostly affects larger microvessels with RBCC diameters of 13 μm or larger. Hence, a more permeable and unstable glycocalyx in the cortical microcirculation is suggested. However, the limited number of included patients reduces the effect of this interesting finding. We found no correlation between sublingual, cortical, and hippocampal PBR values, probably due to the limited number of included patients. When sublingual PBR would be comparable or correlated to cortical and/or hippocampal PBR, the assessment of the sublingual microcirculation would suffice to estimate cerebral glycocalyx 'health'.

To the best of our knowledge, this is the first report on the *in vivo* assessment of the human cerebrovascular glycocalyx. To date, PBR has mainly been evaluated sublingually and has widely been accepted as a valid gauge of glycocalyx health (Dane et al., 2014; Haeren et al., 2016; Martens et al., 2013)

4.5. Relevance of this technique

In this paper, technical details of the assessment of the cerebral microcirculation and its glycocalyx are discussed as a potential tool to study the pathophysiology of underlying chronic drug-resistant epilepsy. Microcirculatory abnormalities in epilepsy patients include altered microvascular density, dysfunctional vessels, and inadequate neurovascular coupling (Heinemann et al., 2012; Kastanauskaite et al., 2009; Parfenova et al., 2005; Rigau et al., 2007). Moreover, increased BBB permeability has been observed in epilepsy patients leading to astrocytic dysfunction and inflammation contributing to the reorganization of the local neuronal network, hyperexcitability, and dysfunctional neurovascular coupling in epilepsy (Heinemann et al., 2012; van Vliet et al., 2014). Since the glycocalyx orchestrates vascular permeability, capillary perfusion, and plasma cell adhesion, it is imperative to further analyze the role of the glycocalyx in the pathophysiology of epilepsy.

Furthermore, alterations in cerebral microvascular structure, neurovascular coupling, and BBB permeability have been implicated to play a role in various neurological disorders, including stroke, dementia, Alzheimer's disease, multiple sclerosis, and Parkinson's disease (Bell and Zlokovic, 2009; Erdő et al., 2017; Martens et al., 2013; Ortiz et al., 2014; Rosenberg, 2012; Zhang et al., 2012). Epilepsy is one of the few chronic neurological disorders in which surgical treatment can be considered, thereby allowing *in vivo* assessment of the cerebral microcirculation and functionally important elements, like the glycocalyx. The current study may therefore contribute to unravel the pathophysiology of epilepsy and other neurological disorders, leading to novel therapeutic approaches. There is still need for this in epilepsy, because an estimated 30–40% of epilepsy patients are drug-resistant (Picot et al., 2008). The development of techniques to assess the cerebral microcirculation and its glycocalyx, as described in this report, is thus highly relevant. Future studies should also be aimed at comparing local cerebral microvascular with retinal microvascular properties. The retina is an easily accessible site of the cerebral microcirculation that can be imaged using non-invasive techniques (Patton et al., 2005).

4.6. Limitations

SDF imaging emits light at a wavelength absorbed by (de)-oxyhemoglobin, visualizing erythrocytes but not the vessel wall. Thus, vessel diameter and glycocalyx health and accessibility are measured indirectly, based on RBCC width variation and PBR, respectively.

Since the aim of this manuscript is technical, the included results are limited to a brief overview of only a few outcome parameters and should be interpreted with caution. Detailed results including a relation to clinical and histopathological parameters will be presented when the study is completed.

5. Conclusion

This is the first report on the *in vivo* assessment of the human cerebrovascular glycocalyx. SDF imaging is a safe, quick, and straightforward technique to evaluate the cerebral microcirculation and its glycocalyx. Since the cerebral microcirculation and its glycocalyx play an eminent role in neurovascular coupling and accommodating cerebral homeostasis, this method may significantly advance research on the pathophysiology of various neurological disorders.

Conflict of interest

This research received no specific grant from any funding agency in the public, commercial or not-for-profit sectors. H. Vink is Chief Science Officer at GlycoCheck BV. There is no financial interest to report.

Ethical statement

All co-authors have seen and agreed with the content of the manuscript. This manuscript has not been submitted to any other journal than *Journal of Neuroscience Methods.* The manuscript has not been published previously. No data has been fabricated or manipulated. No data, text, or theories by others are presented as if they were the author's own. Proper acknowledgments to other works are given.

Author's contribution

R.H.L. Haeren: executive investigator, concept, analysis of data, and drafting manuscript.

K. Rijkers: executive investigator, concept, and critically revising of manuscript.

O.E.M.G. Schijns: executive investigator, epilepsy surgery, and critically revising of manuscript

J. Dings: epilepsy surgery and critically revising of manuscript

G. Hoogland: critically revising of manuscript.

M.A.M.J. van Zandvoort: critically revising of manuscript.

H. Vink: analysis of data, concept and critically revising of manuscript.

J.J. van Overbeeke: supervising investigator, and critically revising manuscript.

Appendix A. Supplementary data

Supplementary data associated with this article can be found, in the online version, at https://doi.org/10.1016/j.jneumeth.2018.03.009.

References

Abbott, N.J., Patabendige, A.A.K., Dolman, D.E.M., Yusof, S.R., Begley, D.J., 2010. Structure and function of the blood–brain barrier. Neurobiol. Dis. 37, 13–25, http://dx.doi.org/10.1016/j.nbd.2009.07.030.

Alonso-Nanclares, L., DeFelipe, J., 2014. Alterations of the microvascular network in the sclerotic hippocampus of patients with temporal lobe epilepsy. Epilepsy Behav. 38, 48–52, http://dx.doi.org/10.1016/j.yebeh.2013.12.009.

Becker, B.F., Chappell, D., Jacob, M., 2010. Endothelial glycocalyx and coronary vascular permeability: the fringe benefit. Basic Res. Cardiol. 105, 687–701, http://dx.doi.org/10.1007/s00395-010-0118-z.

Bell, R.D., Zlokovic, B.V., 2009. Neurovascular mechanisms and blood-brain barrier disorder in Alzheimer's disease. Acta Neuropathol. 118, 103–113, http://dx.doi.org/10.1007/s00401-009-0522-3.

Brown, W.R., Thore, C.R., 2011. Review: cerebral microvascular pathology in ageing and neurodegeneration. Neuropathol. Appl. Neurobiol. 37, 56–74, http://dx.doi.org/10.1111/j.1365-2990.2010.01139.x.

Dane, M.J.C., Khairoun, M.R., Hyun Lee, D., van den Berg, B.M., Eskens, B.J.M., Boels, M.G.S., van Teeffelen, J.W.G.E., Rops, A.L.W.M.M., van der Vlag, J.V., van Zonneveld, A.J., Reinders, M.E.J., Vink, H., Rabelink, T.J., 2014. Association of kidney function with changes in the endothelial surface layer. Clin. J. Am. Soc. Nephrol. 9, 698–704, http://dx.doi.org/10.2215/CJN.08160813.

Dane, M.J.C., van den Berg, B.M., Lee, D.H., Boels, M.G.S., Tiemeier, G.L., Avramut, M.C., van Zonneveld, A.J., Van der Vlag, J., Vink, H., Rabelink, T.J., 2015. A microscopic view on the renal endothelial glycocalyx. Am. J. Physiol. – Ren. Physiol., http://dx.doi.org/10.1152/ajprenal.00532.2014, ajprenal.00532.2014.

de Mesy Bentley, K.L., 2011. An 11-μm-thick glycocalyx?: It's all in the technique! Arterioscler. Thromb. Vasc. Biol. 31, 1712–1713, http://dx.doi.org/10.1161/ATVBAHA.111.229849.

Ebong, E.E., Lopez-Quintero, S.V., Rizzo, V., Spray, D.C., Tarbell, J.M., 2014. Shear-induced endothelial NOS activation and remodeling via heparan sulfate, glypican-1, and syndecan-1. Integr. Biol. (Camb.) 6, 338–347, http://dx.doi.org/10.1039/c3ib40199e.

Erdő, F., Denes, L., de Lange, E., 2017. Age-associated physiological and pathological changes at the blood–brain barrier: a review. J. Cereb. Blood Flow Metab. 37, 4–24, http://dx.doi.org/10.1177/0271678X16679420.

Farrall, A.J., Wardlaw, J.M., 2009. Blood-brain barrier: ageing and microvascular disease–systematic review and meta-analysis. Neurobiol. Aging 30, 337–352, http://dx.doi.org/10.1016/j.neurobiolaging.2007.07.015.

Gould, I.G., Tsai, P., Kleinfeld, D., Linninger, A., 2016. The capillary bed offers the largest hemodynamic resistance to the cortical blood supply. J. Cereb. Blood Flow Metab. 37 (1), 52–68, http://dx.doi.org/10.1177/0271678X 6671146, 0271678X16671146.

Guo, S., Lo, E.H., 2009. Dysfunctional cell–cell signaling in the neurovascular unit as a paradigm for central nervous system disease. Stroke 40, S4–S7, http://dx.doi.org/10.1161/STROKEAHA.108.534388.

Haeren, Van De Ven, S.E.M., Jacobus Van Zandvoort, M.A.M., Vink, H., Van Overbeeke, J.J., Hoogland, G., Rijkers, K., 2016. Assessment and imaging of the cerebrovascular glycocalyx. Curr. Neurovasc. Res., 13, http://dx.doi.org/10.2174/1567202613666160504104434.

Haeren, Vink, H., Staals, J., van Zandvoort, M.A.M.J., Dings, J., van Overbeeke, J.J., Hoogland, G., Rijkers, K., Schijns, O.E.M.G., 2017. Protocol for intraoperative assessment of the human cerebrovascular glycocalyx. BMJ Open 7, e013954, http://dx.doi.org/10.1136/bmjopen-2016-013954.

Heinemann, U., Kaufer, D., Friedman, A., 2012. Blood-brain barrier dysfunction, TGFβ signaling, and astrocyte dysfunction in epilepsy. Glia 60 (8), 1251–1257, http://dx.doi.org/10.1002/glia.22311.

Hunsberger, J.G., Bennett, A.H., Selvanayagam, E., Duman, R.S., Newton, S.S., 2005. Gene profiling the response to kainic acid induced seizures. Mol. Brain Res. 141, 95–112, http://dx.doi.org/10.1016/j.molbrainres.2005.08.005.

Iadecola, C., 2004. Neurovascular regulation in the normal brain and in Alzheimer's disease. Nat. Rev. Neurosci. 5, 347–360, http://dx.doi.org/10.1038/nrn1387.

Jacob, M., Chappell, D., Becker, B.F., 2016. Regulation of blood flow and volume exchange across the microcirculation. Crit. Care, 1–13, http://dx.doi.org/10.1186/s13054-016-1485-0.

Kastanauskaite, A., Alonso-Nanclares, L., Blazquez-Llorca, L., Pastor, J., Sola, R.G., DeFelipe, J., 2009. Alterations of the microvascular network in sclerotic hippocampi from patients with epilepsy. J. Neuropathol. Exp. Neurol. 68, 939–950, http://dx.doi.org/10.1097/NEN.0b013e3181b08622.

Martens, R.J.H., Vink, H., Van Oostenbrugge, R.J., Staals, J., 2013. Sublingual microvascular glycocalyx dimensions in lacunar stroke patients. Cerebrovasc. Dis. 35, 451–454, http://dx.doi.org/10.1159/000348854.

Mathura, K.R., Bouma, G.J., Ince, C., Patterson, J., Bollinger, A., Ince, C., 2001. Abnormal microcirculation in brain tumours during surgery. Lancet 358, 1698–1699, http://dx.doi.org/10.1016/S0140-6736(01)06722-8.

Megens, R.T., Reitsma, S., Schiffers, P.H.M., Hilgers, R.H.P., De Mey, J.G.R., Slaaf, D.W., Egbrink, M.G., Van Zandvoort, M.A., 2007. Two-photon microscopy of vital murine elastic and muscular arteries: combined structural and functional imaging with subcellular resolution. J. Vasc. Res. 44, 87–98, http://dx.doi.org/10.1159/000098259.

Morin-Brureau, M., Lebrun, A., Rousset, M.-C., Fagni, L., Bockaert, J., de Bock, F., Lerner-Natoli, M., 2011. Epileptiform activity induces vascular remodeling and zonula occludens 1 downregulation in organotypic hippocampal cultures: role of VEGF signaling pathways. J. Neurosci. 31, 10677–10688, http://dx.doi.org/10.1523/JNEUROSCI.5692-10.2011.

Muoio, V., Persson, P.B., Sendeski, M.M., 2014. The neurovascular unit – concept review. Acta Physiol. 210, 790–798, http://dx.doi.org/10.1111/apha.12250.

Nieuwdorp, M., Meuwese, M.C., Mooij, H.L., Ince, C., Broekhuizen, L.N., Kastelein, J.J.P., Stroes, E.S.G., Vink, H., 2008. Measuring endothelial glycocalyx dimensions in humans: a potential novel tool to monitor vascular vulnerability. J. Appl. Physiol. 104, 845–852, http://dx.doi.org/10.1152/japplphysiol.00440.2007.

Ortiz, G.G., Pacheco-Moisés, F.P., Macías-Islas, M.Á., Flores-Alvarado, L.J., Mireles-Ramírez, M.A., González-Renovato, E.D., Hernández-Navarro, V.E., Sánchez-López, A.L., Alatorre-Jiménez, M.A., 2014. Role of the blood-brain barrier in multiple sclerosis. Arch. Med. Res. 45, 687–697, http://dx.doi.org/10.1016/j.arcmed.2014.11.013.

Ostrowski, S.R., Berg, R.M.G., Windeløv, N.A., Meyer, M.A.S., Plovsing, R.R., Møller, K., Johansson, P.I., 2013. Coagulopathy, catecholamines, and biomarkers of endothelial damage in experimental human endotoxemia and in patients with severe sepsis: a prospective study. J. Crit. Care 28, 586–596, http://dx.doi.org/10.1016/j.jcrc.2013.04.010.

Pérez-Bárcena, J., Goedhart, P., Ibáñez, J., Brell, M., García, R., Llinás, P., Jiménez, C., Ince, C., 2011. Direct observation of human microcirculation during decompressive craniectomy after stroke. Crit. Care Med. 39, 1126–1129, http://dx.doi.org/10.1097/CCM.0b013e31820ead5e.

Pérez-Bárcena, J., Romay, E., Llompart-Pou, J.A., Ibáñez, J., Brell, M., Llinás, P., González, E., Merenda, A., Ince, C., Bullock, R., 2015. Direct observation during surgery shows preservation of cerebral microcirculation in patients with traumatic brain injury. J. Neurol. Sci. 353, 38–43, http://dx.doi.org/10.1016/j.jns.2015.03.044.

Parfenova, H., Carratu, P., Tcheranova, D., Fedinec, A., Pourcyrous, M., Leffler, C.W., 2005. Epileptic seizures cause extended postictal cerebral vascular dysfunction that is prevented by HO-1 overexpression. Am. J. Physiol. – Heart Circ. Physiol. 288, H2843–H2850, http://dx.doi.org/10.1152/ajpheart.01274.2004.

Patton, N., Aslam, T., MacGillivray, T., Pattie, A., Deary, I.J., Dhillon, B., 2005. Retinal vascular image analysis as a potential screening tool for cerebrovascular disease: a rationale based on homology between cerebral and retinal microvasculatures. J. Anat. 206, 319–348, http://dx.doi.org/10.1111/j.1469-7580.2005.00395.x.

Pennings, F.A., Bouma, G.J., Ince, C., 2004. Direct observation of the human cerebral microcirculation during aneurysm surgery reveals increased arteriolar contractility. Stroke 35, 1284–1288, http://dx.doi.org/10.1161/01.STR.0000126039.91400.cb.

Pennings, F.A., Ince, C., Bouma, G.J., 2006a. The arteriovenous malformation study group: current concepts: arteriovenous malformations of the brain in adults. NEJM 340, 1812–1818, http://dx.doi.org/10.1227/01.NEU.0000243296.69189.B1.

Pennings, F.A., Ince, C., Bouma, G.J., 2006b. Continuous real-time visualization of the human cerebral microcirculation during AVM surgery using orhogonal polarization spectral imaging. Neurosurgery 58, 167–171.

Pennings, F.A., Albrecht, K.W., Muizelaar, J.P., Schuurman, P.R., Bouma, G.J., 2009. Abnormal responses of the human cerebral microcirculation to papaverin during aneurysm surgery. Stroke 40, 317–320, http://dx.doi.org/10.1161/STROKEAHA.108.522375.

Picot, M.C., Baldy-Moulinier, M., Daurès, J.P., Dujols, P., Crespel, A., 2008. The prevalence of epilepsy and pharmacoresistant epilepsy in adults: a population-based study in a Western European country. Epilepsia 49, 1230–1238, http://dx.doi.org/10.1111/j.1528-1167.2008.01579.x.

Pitkänen, A., Lukasiuk, K., 2009. Molecular and cellular basis of epileptogenesis in symptomatic epilepsy. Epilepsy Behav. 14, 16–25, http://dx.doi.org/10.1016/j.yebeh.2008.09.023.

Rahbar, E., Cardenas, J.C., Baimukanova, G., Usadi, B., Bruhn, R., Pati, S., Ostrowski, S.R., Johansson, P.I., Holcomb, J.B., Wade, C.E., 2015. Endothelial glycocalyx shedding and vascular permeability in severely injured trauma patients. J. Transl. Med. 13, 1–7, http://dx.doi.org/10.1186/s12967-015-0481-5.

Reitsma, S., Slaaf, D.W., Vink, H., Van Zandvoort, M.A.M.J., Oude Egbrink, M.G.A., 2007. The endothelial glycocalyx: composition, functions, and visualization. Pflugers Arch. Eur. J. Physiol. 454, 345–359, http://dx.doi.org/10.1007/s00424-007-0212-8.

Rigau, V., Morin, M., Rousset, M.-C., de Bock, F., Lebrun, A., Coubes, P., Picot, M.-C., Baldy-Moulinier, M., Bockaert, J., Crespel, A., Lerner-Natoli, M., 2007. Angiogenesis is associated with blood-brain barrier permeability in temporal lobe epilepsy. Brain 130, 1942–1956, http://dx.doi.org/10.1093/brain/awm118.

Rosenberg, G.A., 2012. Neurological diseases in relation to the blood-brain barrier. J. Cereb. Blood Flow Metab. 32, 1139–1151, http://dx.doi.org/10.1038/jcbfm.2011.197.

Singh, A., Fridén, V., Dasgupta, I., Foster, R.R., Welsh, G.I., Tooke, J.E., Haraldsson, B., Mathieson, P.W., Satchell, S.C., 2011. High glucose causes dysfunction of the human glomerular endothelial glycocalyx. Am. J. Physiol. Renal Physiol. 300, F40–F48, http://dx.doi.org/10.1152/ajprenal.00103.2010.

Taccone, F.S., Su, F., Pierrakos, C., He, X., James, S., Dewitte, O., Vincent, J.-L., De Backer, D., 2010. Cerebral microcirculation is impaired during sepsis: an experimental study. Crit. Care 14, R140, http://dx.doi.org/10.1186/cc9205.

Toth, P., Tarantini, S., Csiszar, A., Ungvari, Z., 2017. Functional vascular contributions to cognitive impairment and dementia: mechanisms and consequences of cerebral autoregulatory dysfunction, endothelial impairment, and neurovascular uncoupling in aging. Am. J. Physiol. – Hear. Circ. Physiol. 312, H1–H20, http://dx.doi.org/10.1152/ajpheart.00581.2016.

Uhl, E., Lehmberg, J., Steiger, H.-J., Messmer, K., 2003. Intraoperative detection of early microvasospasm in patients with subarachnoid hemorrhage by using orthogonal polarization spectral imaging. Neurosurgery 52 (1307), 15–17.

van Vliet, E.A., Aronica, E., Gorter, J.A., 2014. Role of blood-brain barrier in temporal lobe epilepsy and pharmacoresistance. Neuroscience 277, 455–473, http://dx.doi.org/10.1016/j.neuroscience.2014.07.030.

Vlahu, C.A., Lemkes, B.A., Struijk, D.G., Koopman, M.G., Krediet, R.T., Vink, H., 2012. Damage of the endothelial glycocalyx in dialysis patients. J. Am. Soc. Nephrol. 23 (11), 1900–1908, http://dx.doi.org/10.1681/ASN.2011121181.

Wan, Z., Ristagno, G., Sun, S., Li, Y., Weil, M.H., Tang, W., 2009. Preserved cerebral microcirculation during cardiogenic shock. Crit. Care Med. 37, 2333–2337, http://dx.doi.org/10.1097/CCM.0b013e3181a3a97b.

Yoon, J.-H., Lee, E.-S., Jeong, Y., 2017. In vivo imaging of the cerebral endothelial glycocalyx in mice. J. Vasc. Res. 54, 59–67, http://dx.doi.org/10.1159/000457799.

Zhang, J.H., Badaut, J., Tang, J., Obenaus, A., Hartman, R., Pearce, W.J., 2012. The vascular neural network–a new paradigm in stroke pathophysiology. Nat. Rev. Neurol. 8, 711–716, http://dx.doi.org/10.1038/nrneurol.2012.210.